



This is a repository copy of *Finite element modeling of resistive surface layers by micro-contact impedance spectroscopy*.

White Rose Research Online URL for this paper:
<http://eprints.whiterose.ac.uk/156950/>

Version: Published Version

Article:

Veazey, R.A. orcid.org/0000-0001-5827-3771, Gandy, A.S. orcid.org/0000-0003-3692-6211, Sinclair, D.C. orcid.org/0000-0002-8031-7678 et al. (1 more author) (2020) Finite element modeling of resistive surface layers by micro-contact impedance spectroscopy. *Journal of the American Ceramic Society*, 103 (4). pp. 2702-2714. ISSN 0002-7820

<https://doi.org/10.1111/jace.16981>

Reuse

This article is distributed under the terms of the Creative Commons Attribution (CC BY) licence. This licence allows you to distribute, remix, tweak, and build upon the work, even commercially, as long as you credit the authors for the original work. More information and the full terms of the licence here:
<https://creativecommons.org/licenses/>

Takedown

If you consider content in White Rose Research Online to be in breach of UK law, please notify us by emailing eprints@whiterose.ac.uk including the URL of the record and the reason for the withdrawal request.



eprints@whiterose.ac.uk
<https://eprints.whiterose.ac.uk/>

ORIGINAL ARTICLE

Finite element modeling of resistive surface layers by micro-contact impedance spectroscopy

Richard A. Veazey  | Amy S. Gandy  | Derek C. Sinclair  | Julian S. Dean 

Department of Materials Science and Engineering, University of Sheffield, Sheffield, UK

Correspondence

Julian S. Dean, Department of Materials Science and Engineering, University of Sheffield, Sheffield, S1 3JD, UK
Email: j.dean@sheffield.ac.uk

Funding information

Engineering and Physical Sciences Research Council, Grant/Award Number: EP/L015390/1 and EP/L017563/1

Abstract

Micro-contact impedance spectroscopy (MCIS) is potentially a powerful tool for the exploration of resistive surface layers on top of a conductive bulk or substrate material. MCIS employs micro-contacts in contrast to conventional IS where macroscopic electrodes are used. To extract the conductivity of each region accurately using MCIS requires the data to be corrected for geometry. Using finite element modeling on a system where the resistivity of the surface layer is at least a factor of ten greater than the bulk/substrate, we show how current flows through the two layers using two typical micro-contact configurations. This allows us to establish if and what is the most accurate and reliable method for extracting conductivity values for both regions. For a top circular micro-contact and a full bottom counter electrode, the surface layer conductivity (σ_s) can be accurately extracted using a spreading resistance equation if the thickness is ~ 10 times the micro-contact radius; however, bulk conductivity (σ_b) values can not be accurately determined. If the contact radius is 10 times the thickness of the resistive surface, a geometrical factor using the micro-contact area provides accurate σ_s values. In this case, a spreading resistance equation also provides a good approximation for σ_b . For two top circular micro-contacts on thin resistive surface layers, the MCIS response from the surface layer is independent of the contact separation; however, the bulk response is dependent on the contact separation and at small separations contact interference occurs. As a consequence, there is not a single ideal experimental setup that works; to obtain accurate σ_s and σ_b values the micro-contact radius, surface layer thickness and the contact separation must all be considered together. Here we provide scenarios where accurate σ_s and σ_b values can be obtained that highlight the importance of experimental design and where appropriate equations can be employed for thin and thick resistive surface layers.

KEYWORDS

electroceramics, electrodes, finite element analysis, impedance spectroscopy, spreading resistance

This is an open access article under the terms of the Creative Commons Attribution License, which permits use, distribution and reproduction in any medium, provided the original work is properly cited.

© 2019 The Authors. Journal of the American Ceramic Society published by Wiley Periodicals, Inc. on behalf of American Ceramic Society (ACERS)

1 | INTRODUCTION

Impedance spectroscopy (IS) is a versatile technique that is commonly used to extract conductivity values of various electro-active regions in a variety of materials and devices.^{1,2} A particular strength of IS is to identify and probe interfacial phenomena such as resistive grain boundaries or surface layers in addition to the bulk (grain) response in electroceramics.^{3,4} The experiments are usually performed in a two terminal configuration using macroscopic contacts that cover the full surfaces of the sample⁵; however, for local properties to be interrogated, such as a measurement across a single grain boundary, microscopic contacts are required.⁶⁻¹⁰ In each case, the raw data need to be corrected for the electrode/sample geometry using an appropriate model in order to describe how current flows through the material/device. Such corrections become particularly nontrivial when using micro-contacts and can result in significant errors being generated in the measurement of properties if the wrong equation is used. The two most commonly applied corrections to convert a measured resistance (R) into a conductivity (σ) are as follows:

1. a geometric factor using the sample thickness (τ) and electrode area (A):

$$\sigma = \frac{\tau}{RA} \quad (1)$$

2. a spreading resistance, R_{spr} , for a circular micro-contact of electrode radius, r :

$$\sigma = \frac{1}{4rR_{\text{spr}}} \quad (2)$$

For the use of Equation (2) it is assumed there are no resistive extrinsic regions that exist between the micro-contact and counter electrode to block the current.¹¹

Finite element modeling (FEM) is emerging as a useful tool to predict and verify geometric corrections on IS data and to link both electrical and physical microstructures of the system.^{6,12,13} We recently reported the use of FEM to simulate the electrical response of a homogeneous material, for example, a single crystal, using circular micro-contacts in two configurations (top-top and top-bottom) with geometric and spreading resistance corrections.¹⁴ This allowed both the effects of confinement, (electrodes in close proximity to a physical boundary such as the edge of the sample or resistive grain boundary), and contact interference, (electrodes in close proximity to one another), to be investigated. Furthermore, it allowed the conditions

under which to apply either a geometric factor correction or spreading resistance equation to obtain accurate bulk conductivity (σ_b) values. Confinement results in an underestimation of σ_b , whereas for interference it is overestimated. Geometric correction of the data should be used when there is homogeneous current flow through the material, whereas the spreading resistance equation should be used for heterogeneous current flow.

Micro-contact IS (MCIS) can be used to characterize surface layers in materials.¹⁵⁻¹⁷ Work performed by Fleig¹⁵ measured mechanically produced highly conducting surface layers in AgCl using micro-contacts; however, the analysis inferred a surface layer conductivity from changes in the bulk measurement, rather than measuring the surface layer itself. Navickas et al¹⁸ measured yttria-stabilized zirconia thin films (YSZ) (20-90 nm in thickness) on a Silicon substrate by MCIS, in which they used a geometric factor to determine the layer conductivity and the spreading resistance equation to calculate the Si conductivity. The size of the micro-contacts (80-200 μm) were much larger than the thickness of the YSZ layer in this case.

Understanding the properties of surface layers is of interest in many areas of materials science and engineering, for example the study of materials for the nuclear applications whose surfaces are damaged by ion implantation. Generally, these surface layers are thin, typically 1 μm of a 1 mm thick sample (equivalent to ~0.1% of the volume for a sample) and the response from the surface layer is difficult to measure by conventional (full top, full bottom electrodes) IS which obtain measurements across the full sample thickness. Previous investigations^{3,4} have shown a combination of the imaginary components of impedance (Z'') and electric modulus (M'') to be a convenient and effective method to analyze IS data of heterogeneous ceramics, especially in the case for resistive grain boundaries (analyzed using Z'' spectra) and conductive grain cores (analyzed using M'' spectra).

In this script, FEM simulations of circular micro-contacts are extended from our first analysis of a single material to now include a second, more resistive surface layer. This is in direct contact with a relatively more conductive bulk (or substrate) material. The aim is to understand how current flows from contact to contact in such a system and to establish the best method(s) to extract accurate values for the electrical properties of both regions using MCIS. Various scenarios of micro-contacts are simulated, particularly for thicknesses that corresponds to 0.1% of sample volume. These provide guidance for analyzing such data in order to establish the conductivity of the surface layer. This is then extended to thicker surface layers to determine how the method of analysis changes. For this, the IS response of resistive layers that are in the range corresponding to ~1%-50% of sample volume are simulated and the geometric factor and spreading resistance equations used to calculate the conductivity of the surface layer and the bulk, determining the validity and applicability of each equation.

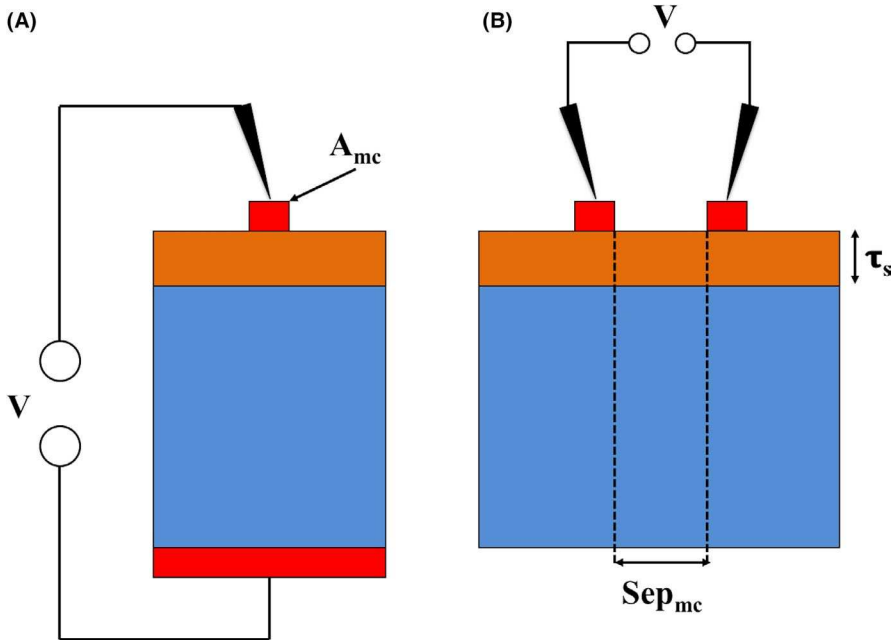


FIGURE 1 Schematic of the circular electrode models for (A) MFTB—micro-contact on the top surface and full contact on the bottom surface, and (B) MTT—two micro-contacts on the same surface. Electrodes are shown in red and this is consistent throughout all figures

2 | MODEL SETUP

Two electrode geometries were investigated: top-bottom and top-top, Figure 1. The bulk was assigned a conductivity $\sigma_b = 13.6 \mu\text{S/m}$ and relative permittivity $\epsilon_r = 162$. These values were determined experimentally by conventional IS measurements with full electrode contacts on a SrTiO_3 single crystal at a temperature of $\sim 300^\circ\text{C}$. The surface layer had the same relative permittivity but its conductivity (σ_s) was lower than the bulk, for example, $\sigma_s = \sigma_b/10$, $\sigma_b/100$, $\sigma_b/1000$. For the top-bottom (cylindrical) geometries, the thickness of the model was set as $100 \mu\text{m}$, where the thickness of the surface layer, τ_s , varied and the bulk making up the difference as $\tau_b = 100 \mu\text{m} - \tau_s$. Electrode contact areas ranged from 1% to 100% coverage of the surface area of the model. For the top-top geometries, a cube of side length $200 \mu\text{m}$ was used with the midpoint between the two contacts defined as the center of the top surface and the electrode contact areas consistent with the top-bottom models. The models presented are simple geometrical representations of more complex systems that occur experimentally. The materials simulated are fully dense, isotropic and homogeneous with no grain boundaries, defects or secondary phases present. The simulations therefore highlight the accuracy of the local contact method under “ideal” conditions. The model set-ups and their validity are described in detail in the Supplementary information (SI) and further details of the FEM code used provided in Ref. [12].

3 | RESULTS

For contacts that cover the full top and bottom surface (FTB), corresponding to conventional IS measurements,

the expected response can be solved analytically because the current flows homogeneously through this model. The resistance, R , and capacitance, C , of each region can be calculated individually and analytically, using Equation (1) and

$$C = \epsilon_0 \epsilon_r \frac{A}{\tau}, \quad (3)$$

respectively, where τ is the thickness of the region, A is the surface area of the electrodes, ϵ_0 is the permittivity of free space and ϵ_r is the permittivity of the material. The magnitude of the Debye peaks in Z'' and M'' spectroscopic plots for each region can be calculated using

$$-Z''_{\max} = \frac{R}{2}, \quad (4)$$

$$M''_{\max} = \frac{1}{2C}. \quad (5)$$

The analytical solutions for a surface layer such that $\sigma_b = 100 \sigma_s$ is shown in Table S1. Simulated Z'' and M'' spectra for FTB models with various surface layer thicknesses are shown in Figure S2 and values calculated, as described above but in reverse order, Table S2. For example, the Z'' and M'' peak maxima values were used to calculate R and C , respectively, using Equations (4) and (5), followed by Equations (1) and (3) to extract conductivity and permittivity, respectively. Additionally, the relationship

$$f_{\max} = \frac{1}{2\pi RC} \quad (6)$$

at the Debye peak maxima was used to extract R (and subsequently σ) and C (and subsequently ϵ_r) from the M'' and Z'' spectra, respectively.

When full surface contacts are used and current flows homogeneously through the model the electrical volume fraction can be easily compared with the physical volume fraction of each material. As both regions have the same surface area and both materials have the same ϵ_r the only factor that determines their physical volume fraction is the thickness of each region. In the first row of Table S1 the physical volume fraction of the surface layer and the bulk is 1 and 99%, respectively. The electrical volume fractions based on calculations using M'' maxima are in agreement with the physical volume fraction. In contrast, the electrical volume fraction does not equal the physical volume fraction based on calculations using Z'' maxima. This is because Z'' is related to the conductivity of the materials, which in this case are different. The calculated electrical volume fractions using Z'' and M'' spectra from the simulated data are compared with the physical volume fractions in Figure S3.

For a FTB model based on $\sigma_b = 100 \sigma_s$ with ϵ_r being the same for both materials, Tables S1 and S2 and Figures S2 and S3 show that M'' spectra are excellent for correlating electrical volume fraction with the physical volume fraction. In contrast, as $\sigma_b = 100 \sigma_s$, Z'' spectra are dominated by the most resistive region. Similar results were obtained for models where $\sigma_b = 1000 \sigma_s$ and $\sigma_b = 10 \sigma_s$. As a consequence, the best form of data analysis for the FTB model is to use Z'' spectra to characterize the resistive surface layer and M'' spectra to characterize the bulk material.

The area of the top contact was then decreased, such that it covered 75, 50, 25, 10, and 1% of the surface of

the model. This created a micro-contact on the top surface while retaining a full-bottom contact (MTFB), Figure 1A. Results for models where $\sigma_b = 100 \sigma_s$ are shown below, however models for $\sigma_b = 1000 \sigma_s$ and $\sigma_b = 10 \sigma_s$ were also simulated and gave similar trends. The results are presented in two different ways. First, fixing the surface layer thickness to monitor the effect of micro-contact size on the IS response, Figure 2, and secondly by fixing the micro-contact size to monitor the effect of surface layer thickness on the IS response, Figure 3.

When the thickness of the surface layer is equal to the bulk, that is, 50 μm , two Debye peaks are resolved in the M'' spectroscopic plots for all contact sizes modeled, Figure 2A. The lower frequency peak is associated with the surface layer response and the higher frequency peak is associated with the bulk response. The M'' response from the surface layer is the same as the bulk for full surface contacts; however, as the size of the top micro-contact decreases, the magnitude of the M'' peak associated with the surface layer increases. In contrast, the M'' response from the bulk is very similar for all micro-contact sizes modeled, suggesting current passes through the bulk in the same manner for any micro-contact size modeled. When the surface layer thickness is 1 μm , the associated M'' Debye peak is small compared with that of the bulk and is difficult to resolve in M'' spectra for larger contact sizes but can be easily resolved when the micro-contact is 5 μm , Figure 2B. In contrast to the larger surface layer thickness, the bulk response increases significantly with decreasing micro-contact size at this surface layer thickness.

When viewing the data in Z'' spectroscopic plots, the spectra are dominated by the resistive surface layer, Figure

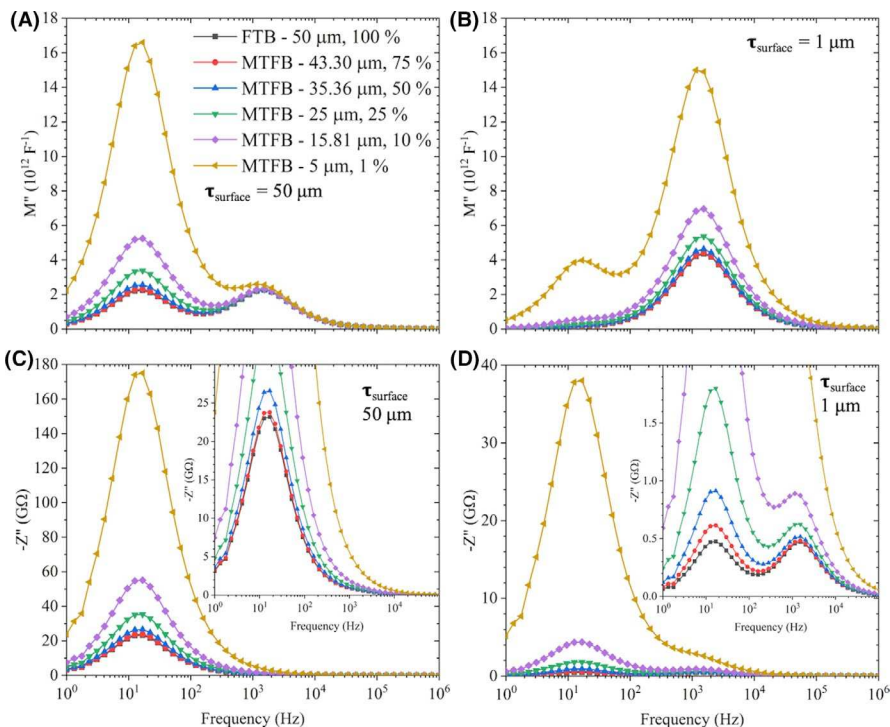


FIGURE 2 M'' and Z'' spectroscopic plots for a 50 μm radius and 100 μm thick cylinder with a surface layer that is 100 times more resistive than the bulk. Surface layer thickness of (A, C) 50 μm and (B, D) 1 μm . MTFB models are labeled by the size of the micro-contact and the percentage surface area. Full top and bottom surface corresponds to 100% surface coverage of the top electrode. The inset of (C) and (D) is the same plot on a smaller Z'' scale to highlight the higher frequency (bulk) response

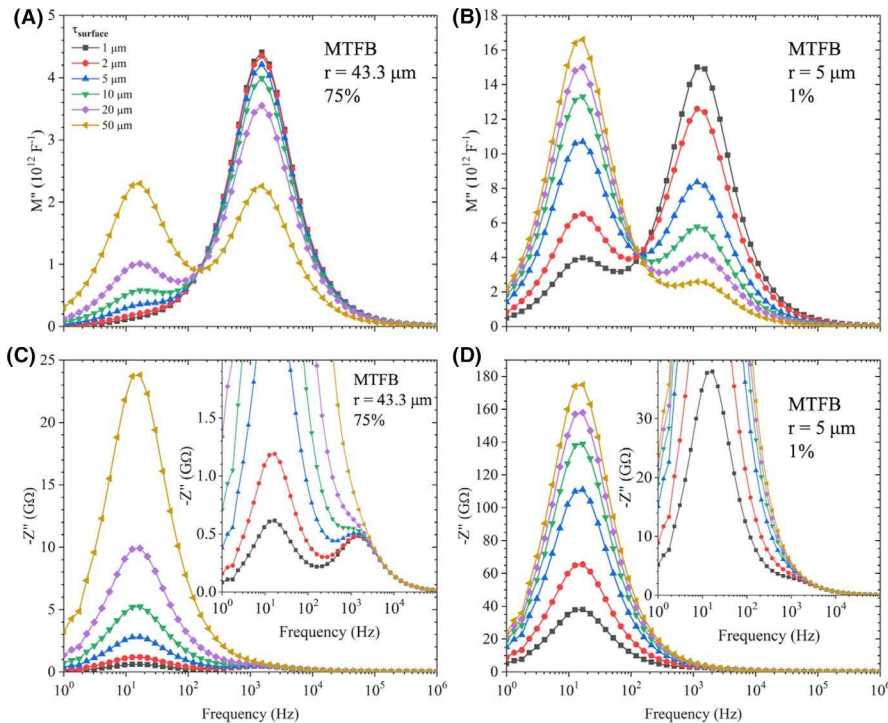


FIGURE 3 M'' and Z'' spectroscopic plots for a 50 μm radius and 100 μm cylinder with a surface layer that is 100 times more resistive than the bulk. The radius of the contact on the top surface is (A, C) 43.3 μm covering 75% of the surface and (B, D) 5 μm covering 1% of the surface. Models are labeled by the surface layer thickness. The inset of (C) and (D) is the same plot on a smaller Z'' scale to highlight the higher frequency (bulk) response

2C and D. The magnitude of both the bulk and surface layer Debye peaks increase as the micro-contact size decreases. It is difficult to resolve the bulk response when the surface layer thickness is 50 μm , Figure 2C, but it can be resolved when the thickness is 1 μm , Figure 2D.

The MCIS data can also be presented by fixing the contact size and changing the surface layer thickness, Figure 3. When the micro-contact radius is 43.3 μm , covering 75% of the surface, Figure 3A, the bulk response dominates the M'' spectroscopic plot for a surface layer thickness of 1 μm . As the thickness of the surface layer increases, its associated M'' peak increases whereas the M'' peak associated with the bulk response decreases. This trend is consistent when the micro-contact radius is reduced to 5 μm , covering 1% of the surface, Figure 3B. When the micro-contact is 5 μm , the M'' response of the surface layer is easier to resolve even for a thickness of 1 μm , emphasizing the localizing effect of micro-contacts, Figure 3B.

As the surface layer thickness increases, its response increases in Z'' spectroscopic plots, Figure 3C and D. The Z'' response from the bulk can be extracted for small surface layer thicknesses and a micro-contact radius of 43.3 μm , Figure 3C, but is more difficult to resolve for smaller micro-contact sizes, Figure 3D, or as the surface layer thickness increases.

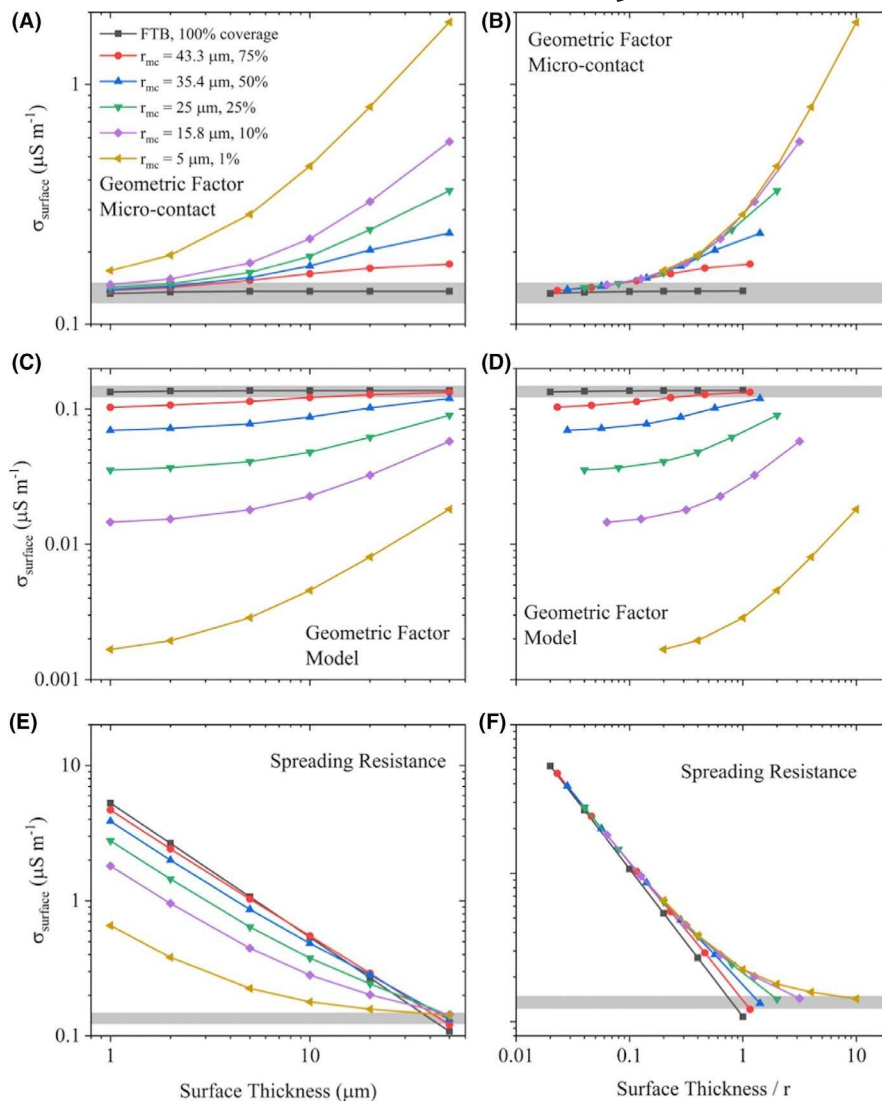
As the micro-contact size decreases, the electrical volume fraction no longer represents the physical volume fraction of the model. Calculated electrical volume fractions of the two regions using Z'' and M'' spectra for the MTFB models are shown in Figure S4. As the size of the top surface electrode decreases (from right to left in Figure S4) the calculated electrical volume fraction from M'' spectra

increases for the surface layer and decreases for the bulk. This highlights the localizing effect that micro-contacts have on electrical measurements, in agreement with our previous results.¹⁴ The calculated electrical volume fractions from Z'' spectra is greatest for the surface layer response for all models. This is attributed to a combination of the surface layer having a conductivity which is 100 times smaller than the bulk and also the localizing effect of the micro-contact.

The conductivities of the bulk and the surface layer were then calculated using both the geometric factor, Equation (1), and the spreading resistance, Equation (2), using the micro-contact surface area and the model surface area, Figure 4. For the surface layer analysis, the resistance values were calculated from the magnitude of the low frequency Z'' peak.

The FTB models (macro-contacts) extract the correct conductivity for the surface layer using the geometric factor. This is true for all thicknesses modeled, see black squares in Figure 4A–D. When the surface layer has a thickness of 1 μm , the geometric factor using the micro-contact area obtains the most accurate approximation of σ_s and is within 10% error for five contact sizes modeled, Figure 4A. When the micro-contact radius is 5 μm , σ_s is not within 10% error but the geometric factor using the micro-contact area still produces a better approximation. If the ratio of the surface layer thickness over the micro-contact radius is <0.1 , σ_s is calculated within 10% error for all models, Figure 4B. The accuracy of the geometric factor using the micro-contact area decreases as the thickness of the surface layer increases.

FIGURE 4 Calculated conductivity of a surface layer that is 100 times more resistive than the bulk for the MTFB models using (A, B) the geometric factor using the micro-contact area, (C, D) the geometric factor using the model area and (E, F) the spreading resistance equation. Each are plotted against the surface layer thickness and the ratio of the thickness over the micro-contact radius. The gray box represents the input conductivity $\pm 10\%$. All values are shown on a log scale



If the geometric factor is instead based on the model area, there is an inaccuracy in σ_s at small thickness. As the surface layer thickness increases the accuracy improves; however, for the thicknesses modeled only the model with a micro-contact radius of 43.3 μm reaches a value within 10% of the input value, Figure 4C and D.

Geometric factors based on the spreading resistance equation leads to an inaccurate estimation of σ_s at small surface layer thicknesses but works well at larger thicknesses, Figure 4E and F. For a micro-contact radius of 5 μm σ_s converges to the input value. The other contact sizes modeled appear to reach a converging limit before continuing to decrease linearly. This is attributed to increased confinement in these models. For example, the FTB case (black squares), which represents a fully confined case, decreases linearly and never converges.

The level of confinement in the model has a significant effect on the calculation of σ_s . In reality, for most MTFB measurements, confinement from the sample size will not be an issue as the micro-contact size will be much smaller

than the sample (eg, for measurements of thin films or single crystals). Figure 5 shows the calculated σ_s using the geometric factor and the spreading resistance equation for the least confined model (micro-contact radius = 5 μm). From this analysis, three general trends emerge: (a) When the surface layer thickness is ~ 10 times smaller than the micro-contact radius, the geometric factor using the micro-contact radius obtains the best approximation of σ_s (black squares in Figure 5). (b) When the surface layer thickness is ~ 10 times greater than the micro-contact radius, the spreading resistance equation obtains the best approximation of σ_s (red circles in Figure 5). (c) The crossover for where either equation is more accurate is at a surface layer thickness that is ~ 0.8 times the micro-contact radius.

Here calculations were also performed for the bulk response and are shown in Figure 6. In this case, the capacitance of the bulk was calculated from the frequency and magnitude of the M'' peak and then converted to resistance, using Equations (5) and (6), respectively.

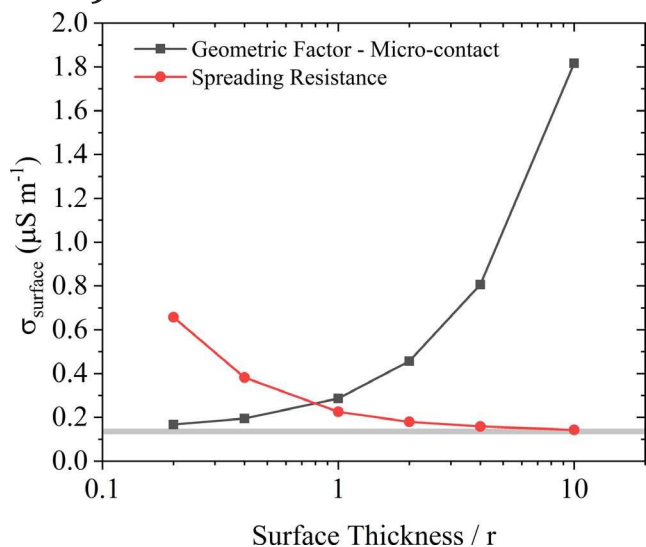


FIGURE 5 Calculated conductivity of a surface layer that is 100 times more resistive than the bulk for the least confined MTFB model (micro-contact radius of 5 μm), using the geometric factor using the micro-contact area or the spreading resistance equation. The gray box represents the input conductivity $\pm 10\%$

The geometric factor using the micro-contact area returns inaccurate σ_b values for all micro-contact sizes modeled and becomes significantly worse as the micro-contact size decreases, Figure 6A and B. The geometric factor using the model area gives the most accurate σ_b values at large surface layer thicknesses for each micro-contact size modeled, Figure 6C and D. Using the spreading resistance, Equation (2), σ_b values converge at small surface layer thicknesses, Figure 6E and F. When the surface layer thickness is small the geometric factor using the micro-contact area gives the best approximation for σ_s , Figure 4A and B.

Analogous plots for the calculated relative permittivity of each region showed similar trends to those for the calculated conductivity and so are not shown here. The permittivity can therefore be calculated to a similar accuracy using the methods discussed above. However, it should be noted that in this study the permittivity of both regions was equal. To test the generality of the results given here, further study of models, where the permittivities are different are required.

Current density plots for a number of the MTFB models where $\sigma_b = 100 \sigma_s$ are shown in Figure 7. When the micro-contact has a radius of 5 μm , covering 1% of the top surface, and the surface layer has a thickness of $\tau_s = 50 \mu\text{m}$, Figure 7A, the current is able to spread out to the full model area within the surface layer. The current flow enters the bulk over an area equal to the full model area and so remains homogeneous throughout the bulk. This is consistent for the larger micro-contact sizes modeled and this surface layer thickness.

When $\tau_s = 10 \mu\text{m}$ and $r_{mc} = 5 \mu\text{m}$, Figure 7B, the current begins to spread out in the surface layer, but the layer is not thick enough for it to fully spread out to the full model area in this layer such as in Figure 7A. The current density in the bulk is inhomogeneous and there is a small amount of spreading from directly underneath the micro-contact. For the same thickness but with a larger contact size of $r_{mc} = 25 \mu\text{m}$, Figure 7C, there is a small amount of spreading again, however, the current density is homogeneous directly underneath the micro-contact.

When $\tau_s = 1 \mu\text{m}$ and $r_{mc} = 5 \mu\text{m}$, Figure 7D and E, the magnitude of the current density in the surface layer significantly decreases away from the micro-contact. The current density in the bulk is inhomogeneous and is spreading from the region directly beneath the micro-contact. This shows similarities to the current density plots for a single material.¹⁴

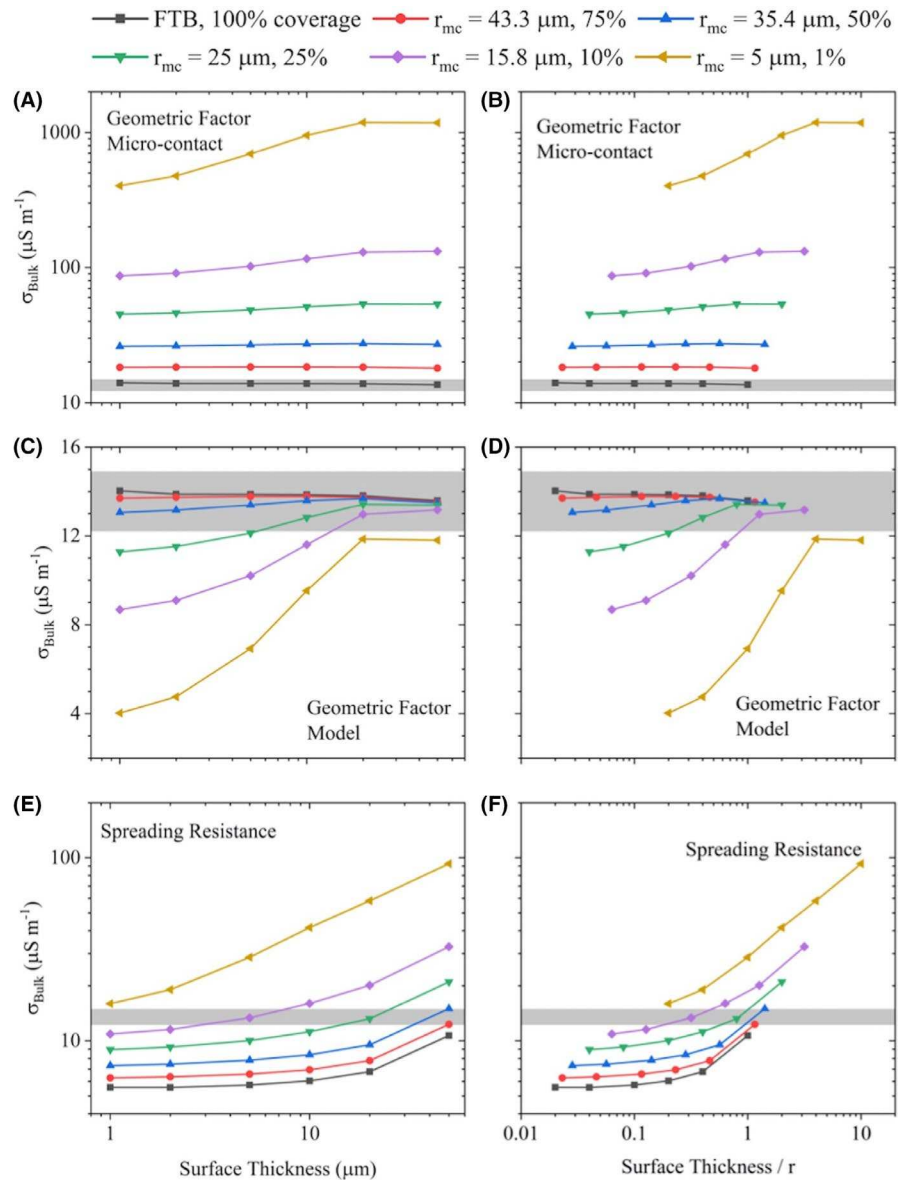
Calculations were then performed for the micro-top-top geometry (MTT), Figure 1B. Simulations set the surface layer to be 10, 100 and 1000 times more resistive than the bulk. Again, similar results were obtained; however, only the results for $\sigma_b = 100 \sigma_s$ are shown for conciseness. The simulated impedance response for a micro-contact radius of 5 μm is shown in Figure 8. The data are again compared by fixing the surface layer thickness and changing the micro-contact separation, Figure 8A and B, and by fixing the contact separation and varying the surface layer thickness, Figure 8C and D.

When the surface layer thickness is fixed at 1 μm and the separation of the micro-contact is varied, the response from the surface layer changes very little in both the M'' and Z'' plots, Figure 8A and B, respectively. This demonstrates the current takes a similar path through the surface layer and is independent of the micro-contact separation. In contrast, the M'' response associated with the bulk increases with increasing separation, Figure 8A, but the changes are difficult to resolve in the Z'' spectra as the surface layer dominates the response, Figure 8B.

For a fixed micro-contact separation, the electrical response changes as a function of the thickness of the surface layer. As the thickness of the surface layer increases, its response increases, whereas the response from the bulk decreases. This is observed in both the M'' and Z'' plots, Figure 8C and D, respectively, as expected. When the thickness of the surface layer is 50 μm (10 times greater than the micro-contact radius), it is difficult to resolve any response from the bulk at all, yellow left triangles in Figure 8C.

The surface conductivity σ_s was extracted using both the spreading resistance equation and the geometric factor based on the micro-contact surface area, Figure 9. For the surface layer analysis, the resistance values were calculated from the magnitude of the low frequency Z'' peaks.

FIGURE 6 Calculated conductivity of the bulk beneath a surface layer that is 100 times more resistive than the bulk for the MTFB models using (A, B) the geometric factor using the micro-contact area, (C, D) the geometric factor using the model area and (E, F) the spreading resistance equation. Each is plotted against the surface layer thickness and the ratio of the thickness over the micro-contact radius. The gray box represents the input conductivity $\pm 10\%$. All values are shown on a log scale



The geometric factor using the micro-contact area provides the best approximation of σ_s if the surface layer thickness is small (filled symbols to the left of plots in Figure 9). As the surface layer thickness increases (moving to the right of plots in Figure 9) the accuracy of this equation decreases. Conversely, the spreading resistance equation overestimates σ_s at small surface layer thicknesses. As the thickness increases, the accuracy of this equation increases (open symbols in Figure 9). The spreading resistance equation becomes a better approximation for σ_s when the surface layer thickness is ~ 0.8 times the micro-contact radius and this is consistent for all micro-contact sizes modeled, Figure 9B, D and F. As the surface layer thickness increases further, the accuracy of using the spreading resistance equation increases and converges to within 10% of the input conductivity.

When the surface layer thickness is less than (or equal to) 0.8 times the micro-contact radius, the calculated σ_s values are independent of separation. In contrast, when the surface layer thickness is >0.8 times the micro-contact radius, the

calculated σ_s values begin to deviate, and are dependent on the separation of the micro-contacts.

The conductivity and relative permittivity were then calculated for the bulk response using the spreading resistance equations and are shown in Figure 10. A geometric factor was not used, as this was shown previously not to be valid for similar types of measurements.¹⁴ In this case, the capacitance of the bulk was calculated from the frequency and magnitude of the M'' peak and then converted to resistance, using Equations (5) and (6), respectively.

The spreading resistance equation returns accurate σ_b values when the surface layer thickness is much smaller than the micro-contact radius, Figure 10A. As the surface layer thickness increases, the accuracy of the spreading resistance equation decreases. A similar trend can be observed for the calculated relative permittivity of the bulk, Figure 10B.

Current density plots for a number of the MTT models where $\sigma_b = 100 \sigma_s$ are shown in Figure 11. When the micro-contact

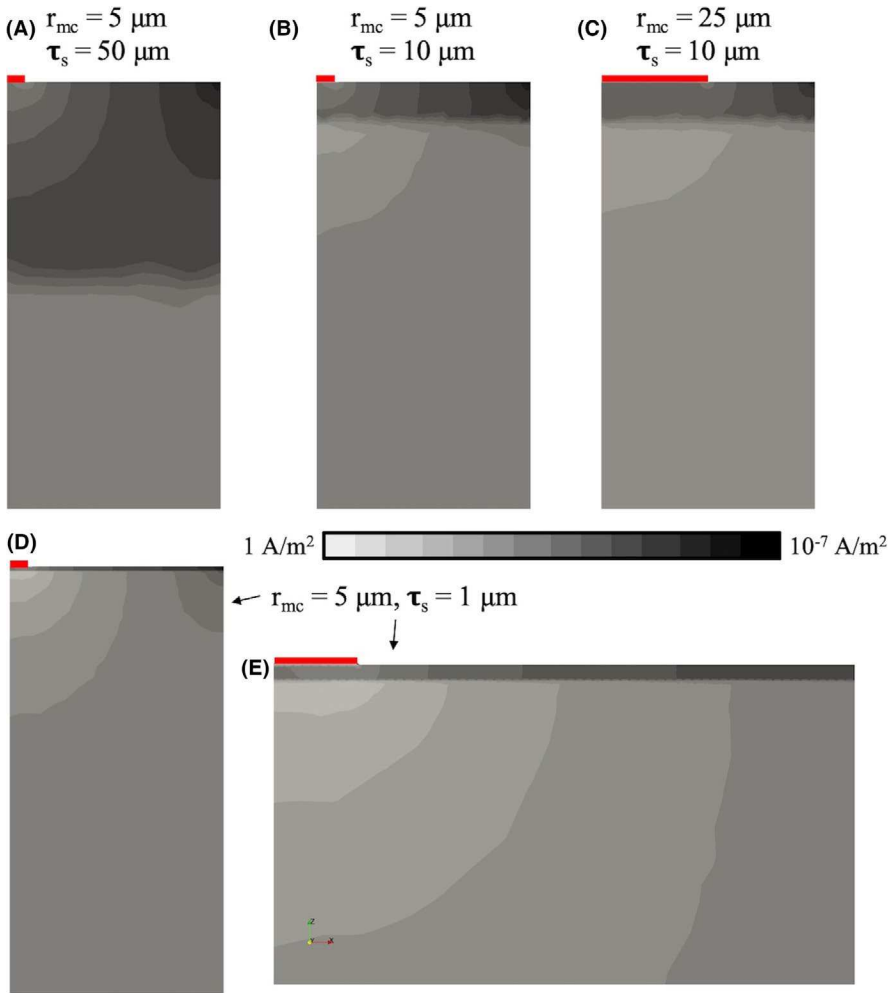


FIGURE 7 Current density plots of a two-layer model using the (quarter) MTFB geometry where the surface layer is 100 times more resistive than the bulk. (A) $r_{mc} = 5 \mu\text{m}$, $\tau_s = 50 \mu\text{m}$, (B) $r_{mc} = 5 \mu\text{m}$, $\tau_s = 10 \mu\text{m}$, (C) $r_{mc} = 25 \mu\text{m}$, $\tau_s = 10 \mu\text{m}$, (D) $r_{mc} = 5 \mu\text{m}$, $\tau_s = 1 \mu\text{m}$, (E) top left corner of (D) on a smaller scale. Black and white represents regions of low and high current density, respectively

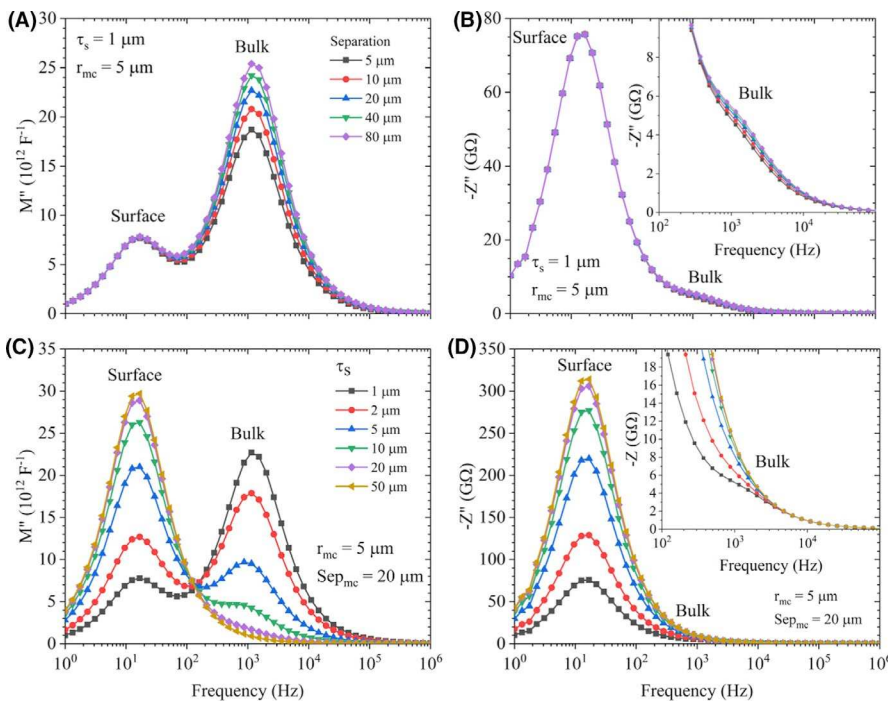


FIGURE 8 Simulated impedance data for a surface layer that is 100 times more resistive than the bulk using the MTT geometry. (A) M'' spectroscopic plots and (B) Z'' spectroscopic plots for a resistive surface layer that is $1 \mu\text{m}$ thick and micro-contact radius of $5 \mu\text{m}$ for a range of contact separations. (c) M'' spectroscopic plots and (d) Z'' spectroscopic plots for a micro-contact radius of $5 \mu\text{m}$ and contact separation of $20 \mu\text{m}$ for a range of surface layer thicknesses

FIGURE 9 Calculated conductivity of a surface layer that is 100 times more resistive than the bulk for the MTT models using the geometric factor using the micro-contact area (solid symbols) or the spreading resistance equation (open symbols). (A, B) micro-contact radius = 2.5 μm , (C, D) micro-contact radius = 5 μm , (E, F) micro-contact radius = 10 μm . s/r in the legend is the ratio of the micro-contact separation over the micro-contact radius. The gray box represents the input conductivity $\pm 10\%$

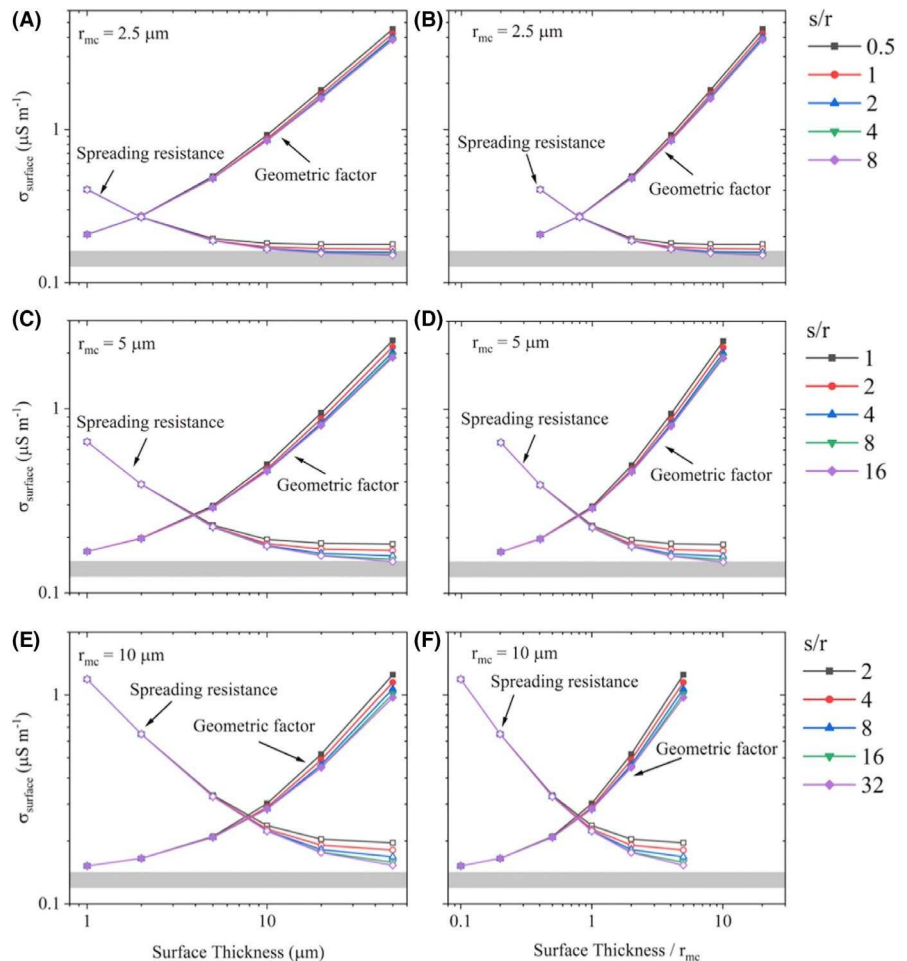
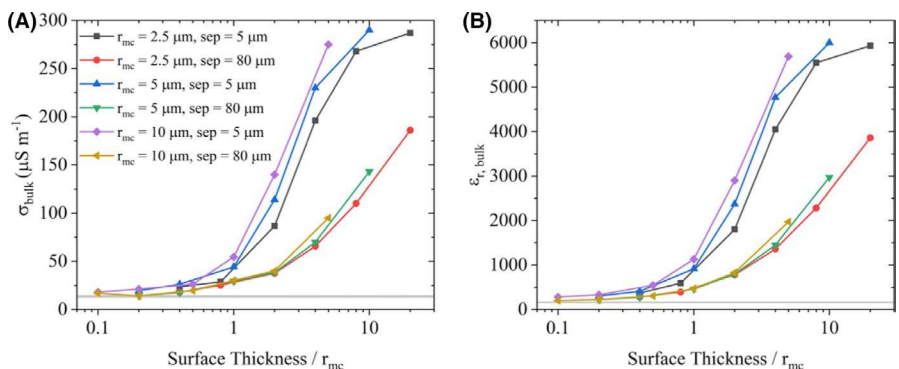


FIGURE 10 (A) Calculated conductivity and (B) relative permittivity for the bulk beneath a surface layer that is 100 times more resistive than the bulk for the MTT models using the spreading resistance equation. The gray box represents the input values $\pm 10\%$



radius is 2.5 μm and the surface layer thickness is 50 μm , the surface layer is sufficiently large for the current to spread out freely and unconfined, Figure 11A. The current density profile in the surface layer is thus very similar to the current density in a single homogeneous material using the MTT geometry.¹⁴

When the micro-contact radius and the surface layer thickness are both 10 μm , shown in Figure 11B, the current begins to spread out in the surface layer but cannot spread out as freely as shown in Figure 11A. This leads to the current density in the bulk being inhomogeneous with some spreading from the regions directly beneath the micro-contacts.

When the micro-contact radius is 5 μm and the surface layer thickness is 1 μm , Figure 11C and D, spreading occurs in the bulk and looks similar to the current density in the surface layer for large thicknesses (Figure 11A) or a single homogeneous material.¹⁴ The current density in the bulk shows the current is spreading from an area that is similar to the micro-contact, Figure 11D.

4 | DISCUSSION

Analytical approaches for current flow in FTB contact geometries is relatively simple due to the homogeneous current

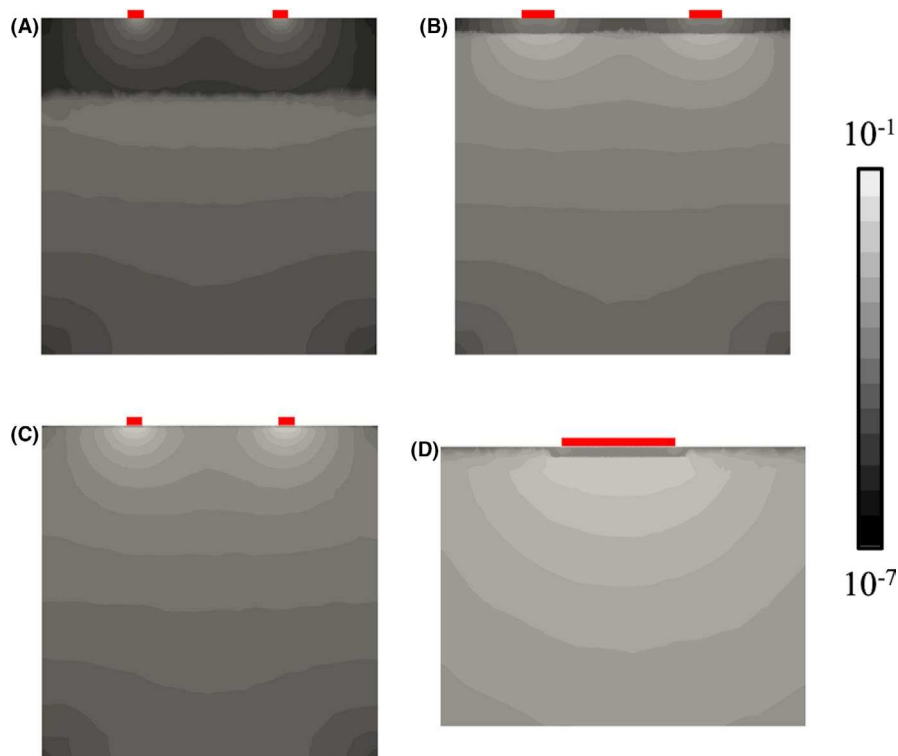


FIGURE 11 Current density plots of a two-layer model using the MTT geometry where the surface layer is 100 times more resistive than the bulk. (A) $r_{mc} = 2.5 \mu\text{m}$, $\tau_s = 50 \mu\text{m}$, separation = $80 \mu\text{m}$, (B) $r_{mc} = 10 \mu\text{m}$, $\tau_s = 10 \mu\text{m}$, separation = $80 \mu\text{m}$, (C) $r_{mc} = 5 \mu\text{m}$, $\tau_s = 1 \mu\text{m}$, separation = $80 \mu\text{m}$, (D) a larger scale image of one of the micro-contacts in (C). Black and white represents regions of low and high current density, respectively. Red represents the micro-contacts. Scale bar is in units of A/m

flow in such systems. This allowed validation of our FEM method and the calculated electrical properties from these simulations (Table S2) and are in agreement with the analytical solution (Table S1). However, when micro-contacts are used, current flow is no longer homogeneous and the approach of using a single analytical solution is difficult.

When using the MTFB geometry, if the surface layer thickness is large, the Z'' and M'' response from the bulk does not change significantly for the different micro-contact sizes modeled, Figure 2A and C. This suggests current flow is similar in this region for each micro-contact size modeled. The current density plot for the smallest micro-contact size modeled ($5 \mu\text{m}$) and a surface layer thickness of $50 \mu\text{m}$, Figure 7A, shows the current flow to be homogeneous throughout the bulk. This is due to the current spreading out completely to fill the model before it reaches the bulk of the model. This will therefore also be true of the larger contact sizes modeled and is the reason why the Z'' and M'' response associated with the bulk does not change significantly with varying micro-contact sizes.

For the model with the least amount of confinement and a micro-contact radius of $5 \mu\text{m}$, the current density spreads from the micro-contact, Figure 7A. Because of this, the spreading resistance equation obtains the best approximation of σ_s , Figure 4F. Due to computational restrictions, this model still has some confinement compared with an experimental sample (such as a surface layer on a single crystal where the confinement could be deemed negligible); however, our results demonstrate if the surface layer thickness is at least 10 times greater than the micro-contact radius, the spreading resistance will produce σ_s values within 10% of the input value, Figure 5.

If the surface layer thickness is similar to the micro-contact radius, calculations of both σ_s and σ_b become difficult, Figures 4 and 6, respectively. The current spreads out in the surface layer but due to confinement cannot spread out as freely as for the thicker surface layer, Figure 7B, causing the accuracy of the spreading resistance equation to reduce. Because the current is spreading out over a larger area than the micro-contact area, the geometric factor using the micro-contact area is also inaccurate, Figure 5. At a surface layer thickness of 0.8 times the micro-contact radius there is a cross-over for which equation is most accurate. At thicknesses greater than this value the spreading resistance equation returns the most accurate values for σ_s . Lower than this value the geometric factor using the micro-contact area returns the most accurate values for σ_s . It is also difficult to calculate σ_b , as it is unknown over what area the current enters the bulk. Where possible, surface layer thicknesses similar to the micro-contact radius should be avoided.

If the surface layer thickness is 10 times smaller than the micro-contact radius the geometric factor using the micro-contact area gives the best approximation of σ_s , Figures 4B and 5. This is because the current is confined and unable to spread out in the limited thickness of the surface layer. This leads to the area the majority of the current passes through the surface layer being similar to the micro-contact area, Figure 7D and E, that is, the majority of the current passes through a cylinder that has length of the surface layer thickness and an area of the micro-contact. The majority of the current enters the bulk over the same area and therefore spreads out from this point, Figure 7D and E; the spreading resistance equation therefore gives the most accurate σ_b , Figure 6F. For the larger micro-contact sizes

modeled, there is a significant amount of confinement, which as explained in Ref. [14], increases the measured resistance and thus an underestimate of σ_b is obtained in this case. Where possible, the micro-contact radius should be at least 10 times the surface layer thickness for accurate conductivities of both the surface layer and bulk to be obtained.

Similar trends can be observed when using two micro-contacts on the same surface (MTT). The crossover where either the geometric factor using the micro-contact area or the spreading resistance equation returns the most accurate σ_s occurs at a surface layer thickness that is 0.8 times the micro-contact radius, Figure 9, consistent with the MTFB results.

If the surface layer thickness is greater than this value, the spreading resistance equation is more accurate, Figure 9. When this is the case, the calculated σ_s is also dependent on the contact separation, as in Ref. [14]. To obtain accurate conductivities one must consider the micro-contact radius, the surface layer thickness and the contact separation. As a consequence, it is difficult to suggest one single ideal experimental setup that would work in all cases.

From Ref. [14] an s/r of 8 for a single, homogeneous material was proposed to obtain conductivities within 10% of the input value. If the micro-contact radius is 10 times smaller than the surface layer thickness, the spreading resistance equation should obtain σ_s values to a similar accuracy. Current density plots, Figure 11A, show the current spreads from the two micro-contacts in a similar way to how spreading occurs in a homogeneous material.¹⁴ The current density in the bulk is inhomogeneous, and greatest near the interface. It is difficult to suggest a geometry that describes this, thus bulk conductivities cannot be calculated with large surface layer thicknesses, Figure 10A.

If the surface layer thickness is smaller than 0.8 times the micro-contact radius, the geometric factor using the micro-contact area returns the most accurate surface layer conductivity, Figure 9, particularly if the thickness is 10 times smaller than the micro-contact radius. When the surface layer thickness is <0.8 times the micro-contact radius, the Z'' and M'' response associated with the surface is independent of contact separation, Figure 8A and B, and in Figure 9 where the data points overlap for the different s/r values modeled. This suggests current takes the same path through the surface layer for all contact separations modeled. The current density in the bulk looks similar to that observed for spreading from two micro-contacts in a homogeneous material, Figure 11C and D, and as such the spreading resistance equation returns the most accurate bulk conductivity, Figure 10A. The bulk response is dependent on the contact separation, Figure 9A and B, in the same way that a homogeneous material is; at small separations, contact interference occurs and therefore conductivity is overestimated.

The results obtained in this study can be summarized in Figure 12 which shows the different contact geometries and the best method for calculation of the respective conductivities when there is no sample confinement. If the surface layer thickness is greater than 10 times the micro-contact radius, the spreading resistance equation should be used to obtain accurate σ_s values, Figure 12A and B. For MTFB, if there is no confinement, σ_b cannot be obtained, Figure 12A, and they cannot be obtained for the MTT case either, Figure 12B.

If the surface layer thickness is at least 10 times smaller than the micro-contact area, the geometric factor using the micro-contact area can be used to obtain accurate σ_s values and the spreading resistance equation can be used to obtain accurate σ_b values, Figure 12C and D.

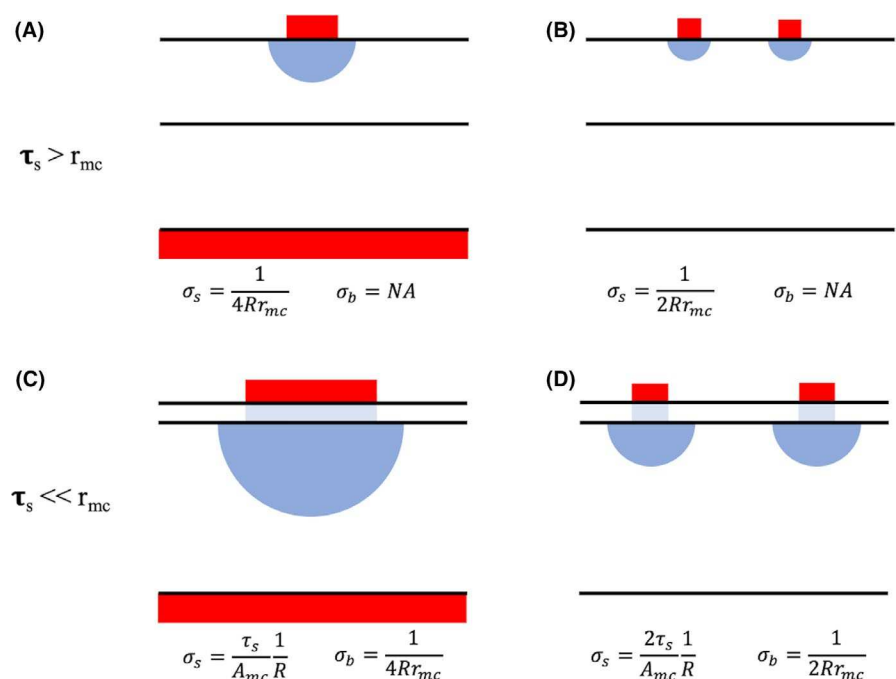


FIGURE 12 (A, C) MTFB and (B, D) MTT contact geometries for an unconfined case when the surface layer thickness is (A, B) greater than the micro-contact radius and (C, D) smaller than the micro-contact radius. The equations to be used to calculate the conductivity of each region is also shown

The materials simulated here are isotropic and homogeneous and the current is confined using a fixed rigid boundary condition, however, experimentally this may not be the case. Work is in progress to simulate the placement of MTT local contacts on a single irregular shaped grain of polycrystalline material which incorporates a “softening” of the current confinement around it. This will allow the significance of conductive grain boundaries and secondary phases on micro contact IS measurements to be assessed.

5 | CONCLUSIONS

The electrical response of a sample with a resistive surface layer has been simulated for different micro-contact geometries. If the thickness of the surface layer is ~10 times larger than the radius of the micro-contact, the spreading resistance equation provides the most accurate approximation of the surface layer conductivity. For an unconfined sample, the conductivity of the bulk cannot be calculated as the area where current enters the bulk remains unknown.

If the thickness of the surface layer is ~10 times smaller than the radius of the micro-contact, the geometric factor using the micro-contact area provides the most accurate approximation of the surface layer conductivity. As a consequence, current enters the bulk over an area that is comparable to the micro-contact radius; therefore, the spreading resistance equation provides the most accurate approximation of the bulk conductivity.

When using two micro-contacts on a thin resistive surface layer, the response from the surface layer is independent of the contact separation. The response from the bulk is dependent on the contact separation and at small separations contact interference occurs, in a similar way to that of a single, homogeneous material.

ACKNOWLEDGMENTS

RAV is supported by the Next Generation Nuclear (NGN) Centre for Doctoral Training at the University of Sheffield, funded by the Engineering and Physical Sciences Research Council, EPSRC, (EP/L015390/1). DCS and JSD thank the EPSRC for financial support (EP/L017563/1).

ORCID

Richard A. Veazey  <https://orcid.org/0000-0001-5827-3771>
 Amy S. Gandy  <https://orcid.org/0000-0003-3692-6211>
 Derek C. Sinclair  <https://orcid.org/0000-0002-8031-7678>
 Julian S. Dean  <https://orcid.org/0000-0001-7234-1822>

REFERENCES

- Irvine JTS, Sinclair DC, West AR. Electroceramics: characterization by impedance spectroscopy. *Adv Mater.* 1990;2(3):132–8.
- Chang BY, Park SM. Electrochemical impedance spectroscopy. *Annual Annu Rev Anal Chem.* 2010;3:207–29.
- Sinclair DC, West AR. Impedance and modulus spectroscopy of semiconducting barium titanate showing positive temperature coefficient of resistance. *J Appl Phys.* 1989;66:3850–6.
- Costa SIR, Li M, Frade JR, Sinclair DC. Modulus spectroscopy of $\text{CaCu}_3\text{Ti}_4\text{O}_{12}$ ceramics: clues to the internal barrier layer capacitance mechanism. *RSC Advances.* 2013;3:7030–6.
- Hwang JH, Kirkpatrick KS, Mason TO, Garboczi EJ. Experimental limitations in impedance spectroscopy: part IV. Electrode Contact Effects. *Solid State Ionics.* 1997;98:93–104.
- Fleig J, Maier J. Point contacts in solid state ionics: finite element calculations and local conductivity measurements. *Solid State Ionics.* 1996; 88:1351–6.
- Lee JS, Fleig J, Maier J, Kim DY, Chung TJ. Local conductivity of nitrogen-graded zirconia. *J Am Ceram Soc.* 2005;88(11):3067–74.
- Rodewald S, Fleig J, Maier J. Measurement of conductivity profiles in acceptor-doped strontium titanate. *J Eur Ceram Soc.* 1999;19:797–801.
- Fleig J, Rodewald S, Maier J. Microcontact impedance measurements of individual highly resistive grain boundaries: general aspects and application to acceptor-doped SrTiO_3 . *J. Appl. Phys.* 2000;87(5):2372–81.
- Rodewald S, Fleig J, Maier J. Microcontact impedance spectroscopy at single grain boundaries in Fe-doped SrTiO_3 polycrystals. *J Am Ceram Soc.* 2001;84(3):521–30.
- Fleig J. Microelectrodes in solid state ionics. In: Alkire RC, Kolb DM, eds. Chapter 1 in *Advances in Electrochemical Science and Engineering.* Weinheim: Wiley-VCH;2002:1–87.
- Dean JS, Harding JH, Sinclair DC. Simulation of impedance spectra for a full three-dimensional ceramic microstructure using a finite element model. *J Am Ceram Soc.* 2014;97(3):885–91.
- Heath JP, Dean JS, Harding JH, Sinclair DC. Simulation of impedance spectra for core-shell grain structures using finite element modeling. *J Am Ceram Soc.* 2015;98(6):1925–31.
- Veazey RA, Gandy AS, Sinclair DC, Dean JS. Modeling the influence of two terminal electrode contact geometry and sample dimensions in electro-materials. *J Am Ceram Soc.* 2019;102:3609–22.
- Fleig J, Maier J. Local conductivity measurements on AgCl surfaces using microelectrodes. *Solid State Ionics.* 1996;85:9–15.
- Fleig J. Microelectrodes in solid state ionics. *Solid State Ionics.* 2003;161:279–89.
- Rupp GM, Opitz AK, Nennung A, Limbeck A, Fleig J. Real-time impedance monitoring of oxygen reduction during surface modification of thin film cathodes. *Nat Mater.* 2017;16:640–5.
- Navickas E, Gerstl M, Friedbacher G, Kubel F, Fleig J. Measurement of the across-plane conductivity of YSZ thin films on silicon. *Solid State Ionics.* 2012;211:58–64.

SUPPORTING INFORMATION

Additional supporting information may be found online in the Supporting Information section.

How to cite this article: Veazey RA, Gandy AS, Sinclair DC, Dean JS. Finite element modeling of resistive surface layers by micro-contact impedance spectroscopy. *J Am Ceram Soc.* 2020;103:2702–2714. <https://doi.org/10.1111/jace.16981>